

# Circumventing spin glass traps by microcanonical spontaneous symmetry breaking

Hai-Jun Zhou<sup>1,2,3</sup>

<sup>1</sup>CAS Key Laboratory for Theoretical Physics, Institute of Theoretical Physics, Chinese Academy of Sciences, Beijing 100190, China

<sup>2</sup>School of Physical Sciences, University of Chinese Academy of Sciences, Beijing 100049, China

<sup>3</sup>Synergetic Innovation Center for Quantum Effects and Applications, Hunan Normal University, Changsha 410081, China

E-mail: zhouhj@itp.ac.cn

**Abstract.** The planted  $p$ -spin interaction model is a paradigm of random-graph systems possessing both a ferromagnetic ground state and an intermediate spin glass phase. Conventional simulated annealing and message-passing algorithms could not reach the planted ground state but are trapped by an exponential number of spin glass states. Here we propose discontinuous microcanonical spontaneous symmetry breaking (MSSB) as a simple mechanism to circumvent all the spin glass traps. The existence of a discontinuous MSSB phase transition is confirmed by microcanonical Monte Carlo simulations. We conjecture that the planted ground state could be retrieved in polynomial time by applying machine-learning methods (such as perceptron-learning) to microcanonically sampled independent configurations. Three candidate algorithms are proposed.

## 1. Introduction

The planted  $p$ -spin interaction model on a finite-connectivity random graph is a representative ferromagnetic system with an intermediate spin glass phase. This model system has played an important role in understanding the physics of structural glasses [1, 2]. This system is also quite relevant and challenging to the field of statistical inference [3, 4]; it is equivalent to the generalized Sourlas code problem in information science [5, 6] and the planted maximum XORSAT problem in computer science [7].

When the environmental temperature slowly decreases, as occurs in a simulated annealing (SA) dynamics [8], the system is predicted to experience an equilibrium phase transition from the disordered paramagnetic phase to the ordered ferromagnetic phase. But this transition never occurs in practice when the interactions are many-body in nature ( $p \geq 3$ ), because the free-energy barrier between these two phases increases exponentially with system size  $N$  and the crystal-nucleation mechanism then simply fails. The system instead remains in the paramagnetic phase as temperature further decreases [1, 2], until finally it is frozen in one of the exponentially many disordered

spin glass states at the bottom of the energy landscape (Fig. 1). Even if the system may occasionally escape from one spin glass state it will soon evolve into another spin glass state, simply because there are so many of such trapping states. Message-passing algorithms based on belief propagation also fail to retrieve the ferromagnetic ground state, even if the objective energy is clamped to values much below those of the spin glass phase [9]. This is because the high gauge symmetry of the planted system makes it statistically indistinguishable from the unplanted purely disordered system [10, 11].

This tremendous computational difficulty is not specific only to the planted  $p$ -spin system but is a common property of many large inference problems such as the planted satisfiability and coloring problems [12, 13, 14]. When the ground state is completely masked by an exponential number of disordered configurations (for example through quiet planting as in the  $p$ -spin system and the coloring problem [14]), and SA and message-passing processes are trapped by spin glass states, it seems the only resort is brute-force enumeration which is of course infeasible even for moderate system sizes  $N$ .

In this work we point out the existence of an alternative route to the planted ground state, namely the route of microcanonical spontaneous symmetry breaking (MSSB). This is a discontinuous transition from the paramagnetic (or disordered symmetric, DS) phase to the microcanonical polarized (MP) phase. The microcanonically stable MP phase has so far been largely overlooked in the literature except for a recent detailed analysis concerning the Potts model [15]. Because the energy density of the system is fixed along the whole DS-to-MP transition trajectory, the difficulty of climbing huge energy barriers is completely avoided (Fig. 1).

The DS and MP phases are connected by many transition trajectories at the given fixed energy density, and therefore ergodicity between these two phases is preserved. The MP phase is entropically favored than the DS phase because it contains exponentially

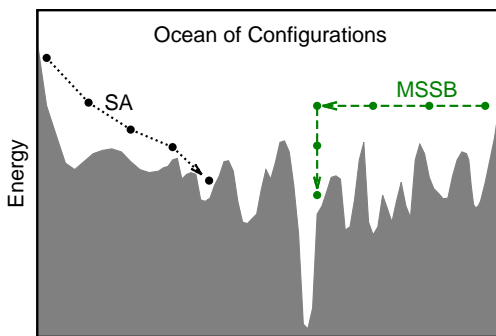


**Figure 1.** An illustration of energy landscape of a planted  $p$ -body interaction spin system ( $p \geq 3$ ). The white region contains all the microscopic configurations of the system. An exponential number of deep local minima (the spin glass states) exist at the bottom of the energy landscape, trapping the simulated annealing dynamics. We propose to take advantage of the discontinuous microscopic spontaneous symmetry breaking which occurs at high energies to directly jump to the basin of attraction of the ground state without encountering spin glass configurations.

more microscopic configurations. Starting from an initial configuration residing in the DS phase, the system is destined to arrive at the MP phase after a sufficiently long waiting time and then reach equilibrium within this phase. The ferromagnetic ground state can then be reached from this intermediate microcanonical phase by gradually decreasing the energy of the system. The MSSB route therefore serves as a conceptually straightforward mechanism to completely circumvent all the low-energy spin glass traps.

We sample a large number of independent microcanonical configurations of the DS phase for the the most studied systems of  $p = 3$  (each interaction involving three vertices) which have the property that their ground state is unique. Very interestingly we find that these DS configurations actually contain information about the unique planted ground state. It may then be possible to infer the planted solution from the sampled DS configurations through machine-learning techniques. We propose three different inference strategies based respectively on the ideas of perceptron-learning, hyperplane optimization, and curve-fitting, to solve the planted  $p$ -spin model. By some simple scaling analysis we conjecture that the planted ground state can be inferred in polynomial time. We hope to be able to confirm this conjecture in the near future by extensive numerical simulations, and then to extend this work to other hard planted systems. Our work also call for theoretical understanding on the interesting asymmetric behavior shown in Fig. 4.

## 2. Theoretical predictions

Consider a planted  $p$ -spin interaction system in which each vertex  $j \in \{1, \dots, N\}$  participates in  $K$  interactions (clauses) and each clause involves  $p$  randomly chosen vertices (we set  $p=3$  in all the following numerical computations). The total number of clauses is  $M=KN/p$ . The energy of a generic configuration  $\vec{\sigma} \equiv (\sigma_1, \dots, \sigma_N)$  is

$$E(\vec{\sigma}) = - \sum_{a=1}^M J_a \prod_{j \in \partial a} \sigma_j , \quad (1)$$

where  $\sigma_j \in \pm 1$  is the spin of vertex  $j$  and  $\partial a$  denotes the set of vertices constrained by clause  $a$ . We denote by  $u$  the energy density of the system, namely

$$u = \frac{E(\vec{\sigma})}{N} . \quad (2)$$

There is a planted spin configuration  $\vec{\sigma}^0 \equiv (\sigma_1^0, \dots, \sigma_N^0)$  dictating the coupling constant of clause  $a$ , such that

$$J_a = \begin{cases} + \prod_{j \in \partial a} \sigma_j^0 & \text{(probability } 1 - \varepsilon) , \\ - \prod_{j \in \partial a} \sigma_j^0 & \text{(probability } \varepsilon) . \end{cases} \quad (3)$$

The parameter  $\varepsilon$  is the noise level of the above planting rule. When  $\varepsilon > 0$  model (1) can then be interpreted as the Sourlas code of  $p$ -body interactions [5, 6]. When  $\varepsilon$  is

sufficiently small the planted configuration  $\vec{\sigma}^0$  is a ground state of Eq. (1) and it may lie extensively below all the other minimum-energy configurations (Fig. 1). We define the overlap (magnetization)  $m$  of configuration  $\vec{\sigma}$  with respect to  $\vec{\sigma}^0$  as

$$m = \frac{1}{N} \sum_{j=1}^N \sigma_j \sigma_j^0. \quad (4)$$

This random-graph system has been intensively studied by the mean-field cavity method of statistical mechanics [16, 17, 10, 18]. The mean-field results obtained at  $\varepsilon = 0$  and  $K = 10$  are demonstrated in Fig. 2, and the qualitatively identical results obtained for  $K = 4$  are shown in Fig. A1 (Appendix A). Some aspects of these theoretical results are similar to what were found for the Potts model [15], but there is a key qualitative difference to be discussed at the end of this section. First, let us interpret these

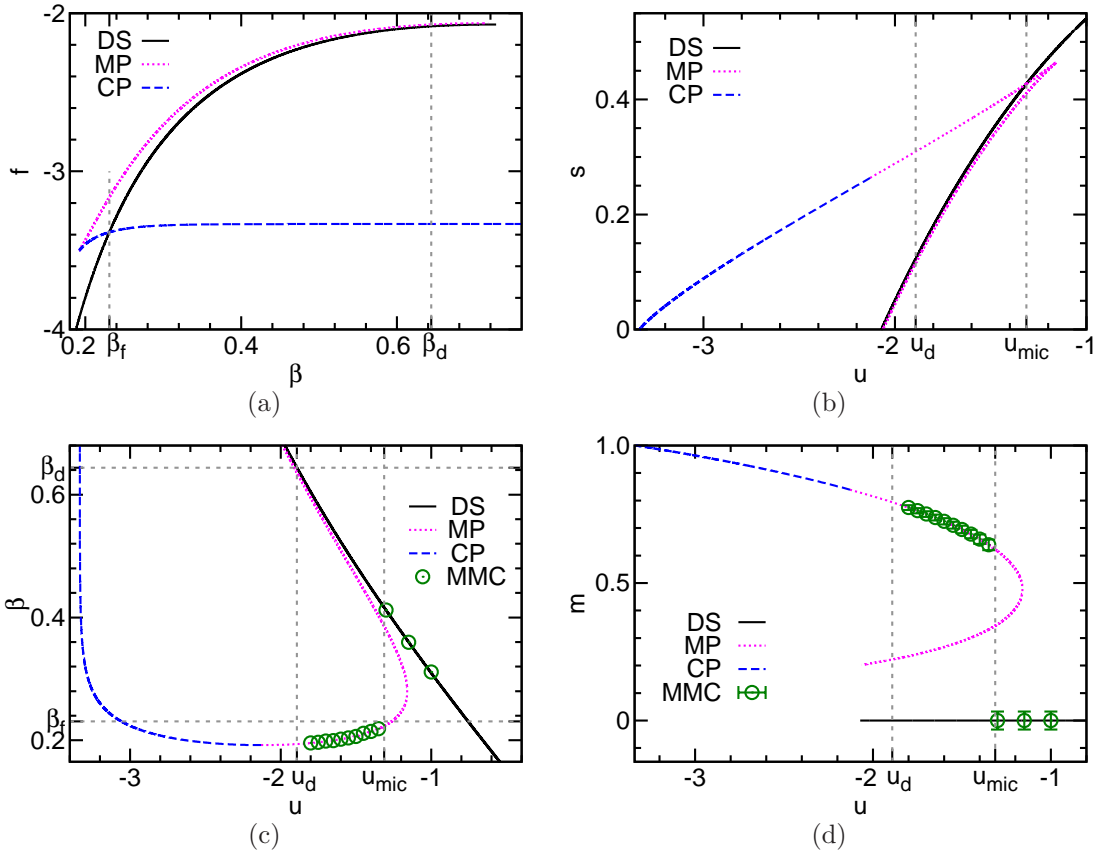


**Figure 2.** The DS (solid lines), MP (dotted lines), and CP (long dashed lines) fixed points of the mean-field theory for the planted 3-body model on random graphs of degree  $K = 10$  at noise  $\varepsilon = 0$ . (a) Free energy density  $f$  versus canonical inverse temperature  $\beta$ . (b) Entropy density  $s$  versus energy density  $u$ . (c) Microcanonical inverse temperature  $\beta$  versus  $u$ . (d) Mean overlap  $m$  versus  $u$ .  $\beta_d$  and  $u_d$ : critical inverse temperature and energy density at the dynamical SG phase transition;  $u_{\text{mic}}$ : critical energy density at the MSSB phase transition;  $\beta_f$ : critical inverse temperature at the canonical ferromagnetic phase transition. The predicted MSSB phase transition is confirmed by MMC simulations (circles) on a single problem instance of size  $N = 960$ .

theoretical predictions from the perspective of microcanonical thermodynamics [19].

The configuration space has a disordered symmetric phase whose mean magnetization is zero in the thermodynamic limit. This DS phase contains the paramagnetic spin configurations. As the energy density  $u$  decreases to the spin glass (SG) dynamical transition point  $u_d$  this DS phase suddenly divides into an exponential number of ergodicity-broken macro-states, and the system then enters into the SG phase [1]. The value of  $u_d$  is independent of  $\varepsilon$  because of gauge symmetry [10] and can be determined by the tree-reconstruction method [17] (see also textbooks [4, 18]). Because of planting, a stable canonical polarized (CP) phase containing configurations similar to  $\vec{\sigma}^0$  exist in the configuration space at sufficiently low energies. This CP phase is simply the conventional ferromagnetic phase.

The Microcanonical polarized phase, corresponding to the unstable fixed point of the mean field theory with higher free energy density [Fig. 2(a)], serves as the watershed between the DS and CP phases [Fig. 2(c)]. Configurations of the MP phase have positive magnetizations and therefore are similar to  $\vec{\sigma}^0$ , but they are unstable in the canonical ensemble. The MP phase can only be explored by fixing the energy density  $u$ .

The entropy density  $s$  of the MP phase as a function of energy density  $u$  has two branches [Fig. 2(b)]. The higher-entropy branch corresponds to the MP configurations that are stable at fixed  $u$ , and its entropy starts to surpass that of the DS phase at the critical energy density  $u_{\text{mic}}$ , indicating a discontinuous microcanonical spontaneous symmetry-breaking phase transition. This transition leads to a jump in the mean magnetization and a drop in the microcanonical inverse temperature  $\beta$ , which are verified by our simulation results [Figs. 2(c) and 2(d)]. The lower-entropy MP branch, on the other hand, always has lower entropy than that of the DS phase; it marks the watershed between the MP and DS phases in the microcanonical ensemble.

We observe that the MSSB transition energy density  $u_{\text{mic}}$  is located above the SG transition point  $u_d$  when the noise level  $\varepsilon$  is low enough (Table 1). In principle it is then possible to reach the MP phase by inducing a MSSB transition at fixed value of  $u \in (u_d, u_{\text{mic}})$ , avoiding the spin glass traps of the canonical ensemble. We will continue to discuss the practical feasibility of this proposal in the next two sections. A relevant observation to this issue is that the DS fixed point of the  $p$ -spin model is always locally

**Table 1.** Magnetization jump  $\Delta m$ , microcanonical inverse temperature drop  $\Delta \beta$ , critical energy density  $u_{\text{mic}}$ , at the MSSB phase transition of the planted 3-body model on random graphs of degree  $K$  (noise  $\varepsilon = 0$ ). The critical energy densities  $u_d$  are also listed (based on Table 4.2 of [18]).

$K$	4	5	6	7	8	9	10
$\Delta m$	0.906	0.821	0.758	0.712	0.676	0.647	0.623
$\Delta \beta$	-0.595	-0.409	-0.324	-0.274	-0.239	-0.214	-0.193
$u_{\text{mic}}$	-1.115	-1.167	-1.204	-1.235	-1.264	-1.289	-1.313
$u_d$	-1.159	-1.316	-1.453	-1.575	-1.687	-1.792	-1.892

stable, down to the minimal energy density at which the entropy density becomes zero [Fig. 2(b)]. Consequently a gap of the overlap  $m$  always exists between the DS and MP phases down to this minimal energy density [Fig. 2(d)]. This feature is significantly different from what was observed in the Potts model (Fig. 2(d) of Ref. [15]). The DS phase of the Potts model becomes unstable below certain threshold energy density. By fixing the energy density below this threshold value, the system will then evolve from the DS phase to the MP phase gradually. Such a gradual evolution will not be possible for the  $p$ -spin model because of the gap in the order parameter  $m$ .

### 3. Microcanonical Monte Carlo

We implement a simple MMC dynamics to explore configurations at the vicinity of an objective energy  $E_o \equiv Nu$  with  $u \in (u_d, u_{\text{mic}})$ . After the system reaches  $E_o$  from a random initial configuration through SA or irreversible energy diving, we keep updating its configuration  $\vec{\sigma}$  by single-spin flips. An elementary MMC trial consists of picking a vertex  $j$  uniformly at random, proposing a flip  $\sigma_j \rightarrow -\sigma_j$ , and accepting this flip if the new configuration energy does *not* exceed  $E_o$ . We sample configurations at fixed intervals and record their overlap values and energies. The microcanonical inverse temperature is estimated through

$$\beta = \frac{1}{4} \ln \left( 1 + \frac{4}{E_o - \langle E(\vec{\sigma}) \rangle} \right), \quad (5)$$

where  $\langle E(\vec{\sigma}) \rangle$  is the averaged energy of the configuration samples [20].

Our MMC dynamics is an unbiased and ergodic random walk within the microcanonical configuration space. As evolution time goes to infinity every configuration of this space has equal frequency to be visited, and then the system will certainly be in the MP phase as this phase is exponentially dominant in statistical weight. Empirically we have observed that this MMC dynamics achieves MSSB in small-sized systems [Fig. 3(b)]. It is more easier for the MSSB transition to occur in networks of larger degrees  $K$ . This is consistent with the mean-field theoretical results, which reveal that the entropy barrier and the gap of the order parameter  $m$  both decreases with  $K$  (Table 1). The hardest RR problem instances are those with degree  $K=4$ .

But when  $N$  becomes larger ( $N > 350$  for  $K=4$ ,  $N > 2000$  for  $K=10$ , and  $N > 4000$  for  $K=20$ ) the waiting time needed to observe a MSSB transition starts to increase exponentially with  $N$ . This slowing down is due to an entropy-barrier effect [Fig. 3(a)].

On the coarse-grained level the MMC dynamics is a one-dimensional random walk under a potential field  $-s_u(m)$ , where  $s_u(m)$  is the entropy density of configurations at energy density  $u$  having overlap  $m$  with the planted configuration  $\vec{\sigma}^0$ . At each elementary trial,  $m$  may change to  $m \pm 2/N$  with probability proportional to  $(1 \mp g_m)/2$ . The bias ratio is

$$g_m = \frac{1 - e^{2s'_u(m)}}{1 + e^{2s'_u(m)}}, \quad (6)$$

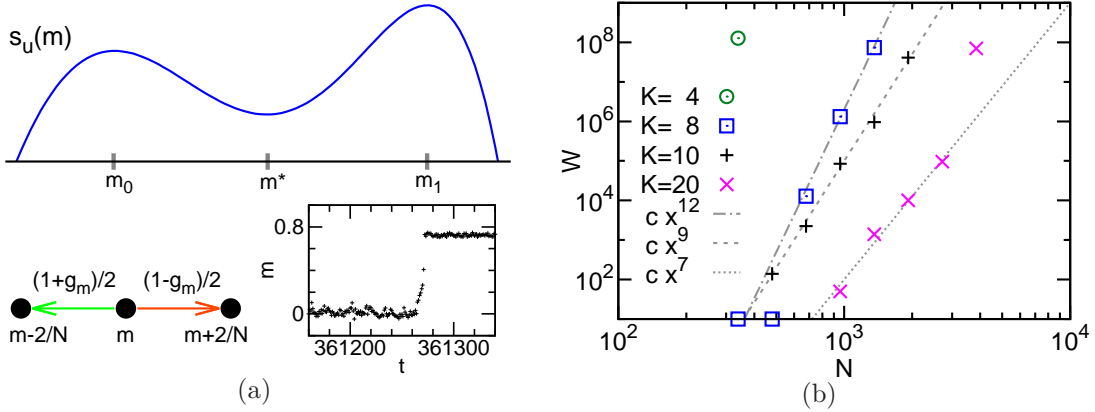


**Figure 3.** The time complexity of observing a MSSB transition. (a) A schematic curve of the entropy density  $s_u(m)$  of the planted 3-body model at fixed energy density  $u$  and noise  $\epsilon = 0$ , showing a local maximum at overlap  $m_0 \approx 0$ , a global maximum at  $m_1$ , and a minimum at  $m^*$ . The MMC dynamics is equivalent to a one-dimensional biased random walk with bias ratio  $g_m$ . The example evolution trajectory shows a MSSB event at  $u = -1.61$  in a random graph of degree  $K = 10$  and size  $N = 960$  (one unit of MMC time  $t$  means  $N$  spin-flip trials). (b) The simulated waiting time  $W$  for single problem instances. Each point is obtained by simulating 24 independent MMC evolution trajectories on a single network and then setting  $W$  to be the length of the shortest trajectory:  $K = 4$ ,  $u = -1.133$  (circle);  $K = 8$ ,  $u = -1.6$  (squares);  $K = 10$ ,  $u = -1.61$  (pluses);  $K = 20$ ,  $u = -2.2$  (crosses). Lines are power-law  $cN^b$  reference relations.

with  $s'_u(m) \equiv ds_u(m)/dm$  being the slope of  $s_u(m)$  at  $m$ . Because  $s'(m) < 0$  in  $m \in (0, m^*)$  with  $m^*$  being the watershed point of  $s_u(m)$ , the occurrence of MSSB is an exponentially rare first-passage event characterized by a waiting time of order  $O(e^{N[s_u(0)-s_u(m^*)]})$  [21, 22].

#### 4. Asymmetry of overlap distribution

When  $p$  is odd so that each clause of the energy (1) involves an odd number of vertices, the planted configuration  $\vec{\sigma}^0$  is a ground state of the system but the globally flipped one  $(-\vec{\sigma}^0)$  is not. Furthermore,  $\vec{\sigma}^0$  will be the unique ground state if  $K \geq 4$  and the clause number  $M$  is not too small. We conceive that since the entropy density  $s_u(m)$  is “M”-shaped with a minor peak at  $m \approx 0$  and a major peak at a positive overlap [Fig. 3(a)], it should *not* be strictly symmetric in the vicinity of  $m = 0$  when  $N$  is finite. Instead, for relatively large overlap magnitudes,  $s_u(+|m|)$  may slightly exceed  $s_u(-|m|)$ . As the probability  $P(m)$  of observing an overlap value  $m$  is related to  $s_u(m)$  by  $P(m) \propto e^{Ns_u(m)}$ , we can quantify the magnitude of entropy asymmetry by examining the  $P(m)$  profile. Some representative simulation results for  $p = 3$  are shown in Fig. 4 and in Fig. A3 (Appendix A).

Consistent with our expectations, the overlap  $m$  is more likely to be positive when  $|m| > 1.75N^{-\frac{1}{2}}$ . On the other hand we were initially quite puzzled to notice that  $m$

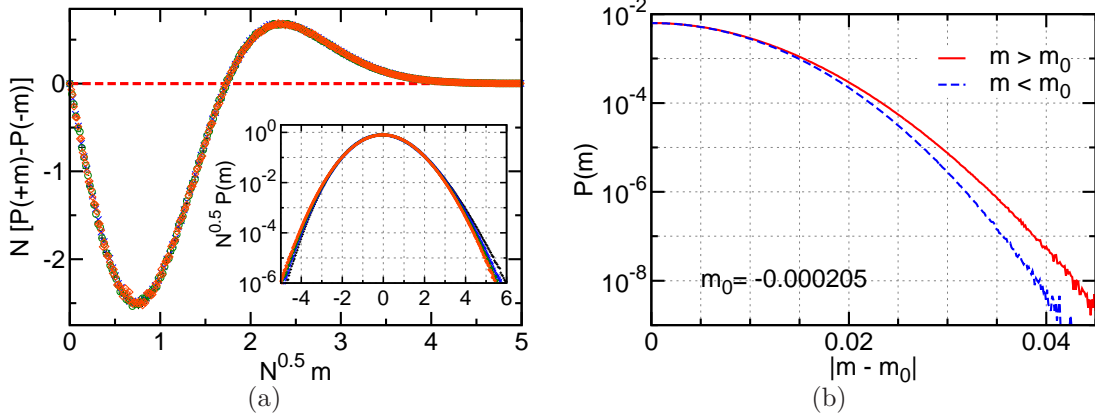


**Figure 4.** Asymmetry of the overlap distribution  $P(m)$  for the planted 3-body model at noise  $\varepsilon=0$ . (a) Rescaled probability difference  $N[P(+|m|) - P(-|m|)]$  versus rescaled overlap  $\sqrt{N}m$  for a single random-graph system of degree  $K=4$  at  $u=-1.135$ : size  $N=2004$  (pluses), 4008 (crosses), 8016 (circles), and 16032 (squares). The inset shows  $\sqrt{N}P(m)$  versus  $\sqrt{N}m$ . (b) The two branches of  $P(m)$  at  $m > m_0$  and  $m < m_0$  for the system of size  $N=16032$ , with  $m_0=-0.000205$  being the most probable overlap value.

is significantly biased toward negative values for smaller values of  $|m|$ , especially at  $|m| \approx 0.75N^{-\frac{1}{2}}$ . After some detailed analysis we now understand that this peculiar behavior is caused by the fact that the most probable overlap value (denoted as  $m_0$ ) of the distribution  $P(m)$  is not located exactly at zero but is slightly negative ( $m_0 < 0$ ). After correcting for this slight shift we find that the probability distribution  $P(m)$  is systematically biased towards the positive side of  $m_0$  than towards the negative side [Fig. 4(b)].

The numerical results of Fig. 4(a) and Fig. A3 also reveal that the histograms for different system sizes roughly superimpose onto each other after rescaling  $P(m)$  by  $N^{-1}$  and  $m$  by  $N^{-\frac{1}{2}}$ . From this scaling behavior we infer that the probabilities of overlap  $m$  being non-positive ( $p_{\leq 0}$ ) and non-negative ( $p_{\geq 0}$ ) change with  $N$  as

$$p_{\leq 0} = \frac{1}{2} + \frac{\gamma}{2}N^{-\frac{1}{2}}, \quad p_{\geq 0} = \frac{1}{2} - \frac{\gamma}{2}N^{-\frac{1}{2}}, \quad (7)$$

and the mean and squared-mean overlaps decay with  $N$  according to

$$\langle m \rangle = \mu N^{-1}, \quad \langle m^2 \rangle = N^{-1}. \quad (8)$$

The values of the asymmetry coefficients  $\gamma$  and  $\mu$  are determined by two competing effects, namely that the most probable overlap value  $m_0$  is negative and that  $P(m_0 + |\Delta m|) > P(m_0 - |\Delta m|)$  for any deviation  $\Delta m$  of overlap from  $m_0$ . We expect that these two coefficients  $\gamma$  and  $\mu$  are distinct from zero in general. Given a problem instance, we can estimate  $\gamma$  and  $\mu$  by MMC assuming  $\vec{\sigma}^0 = (1, \dots, 1)$ . For example, we estimate that  $\gamma = 0.9070 \pm 0.0007$  and  $\mu = 0.0066 \pm 0.0007$  for the single problem instance of degree  $K=4$  and size  $N=4008$  at  $u=-1.135$  of Fig. 4(a), by averaging over  $7.5 \times 10^9$  configuration samples through the bootstrap method (Appendix B).

The asymmetry of the overlap probability distribution  $P(m)$  persists even when the energy density  $u$  is higher than the MSSB phase transition value  $u_{\text{mic}}$ . This fact is demonstrated in Fig. A2 (Appendix A) by MMC simulation results obtained at different energy densities  $u$  on a single RR network instance of size  $N=4008$  and degree  $K=4$ . Therefore the condition  $u < u_{\text{mic}}$  is not strictly necessary to explore the asymmetry of  $P(m)$ . Of course the extend of asymmetry in  $P(m)$  decreases as  $u$  increases, and  $P(m)$  should be perfectly symmetric at  $u=0$ .

## 5. Inference on microcanonical configuration samples

Equation (7) indicates that a single configuration sample  $\vec{\sigma}$  contains  $O(N^{-\frac{1}{2}})$  bit information about the planted configuration  $\vec{\sigma}^0$ . It may then be possible to infer  $\vec{\sigma}^0$  directly from a sufficiently large number of configurations sampled at fixed energy density  $u$ , without waiting for a rare MSSB transition event. Here we discuss three different inference strategies.

### 5.1. Perceptron-learning

Assuming  $\mu$  of Eq. (8) to be non-zero, we may construct a perceptron-learning problem to infer  $\vec{\sigma}^0$  (stragegy A). The recipe is quite straightforward. We sample  $Q$  independent configurations  $\vec{\sigma}(t)$  at equal time intervals, here  $t$  is the index of a sampled configuration, and then add them together to form a composite vector  $\vec{r} \equiv (r_1, \dots, r_N) = \sum_{t=1}^Q \vec{\sigma}(t)$ . Define the alignment  $L$  between  $\vec{r}$  and  $\vec{\sigma}^0$  as  $L \equiv \sum_{i=1}^N r_i \sigma_i^0$ . Because of Eq. (8) the random variable  $L$  follows approximately a Gaussian distribution with mean  $\mu Q$  and standard deviation  $\sqrt{NQ}$ . Therefore if setting  $Q$  to be proportional to  $N$  with  $Q \geq (5/\mu)^2 N$  then the signs of  $L$  and  $\mu$  will highly likely be the same. As an example, this number is  $Q \approx 2.3 \times 10^9$  for the problem instance of size  $N=4008$  and degree  $K=4$  in Fig. 4(a). After getting a large number  $X$  of such indendent composite vectors by parallel computing [28], we can feed them to a perceptron to infer  $\vec{\sigma}^0$ .

The inferred probability  $P_A(\vec{\sigma}^0)$  of the planted configuration being  $\vec{\sigma}^0$  in this perceptron-learning task is

$$P_A(\vec{\sigma}^0) \propto \prod_{\ell=1}^X \Theta\left(\theta_\mu \sum_{i=1}^N r_i^{(\ell)} \sigma_i^0\right), \quad (9)$$

where  $\Theta(x)$  is the Heaviside function with  $\Theta(x) = 1$  for  $x > 0$  and  $\Theta(x) = 0$  for  $x \leq 0$ , and  $r_i^{(\ell)}$  is the  $i$ -th entry of the  $\ell$ -th composite sample vector [23, 24, 25, 26, 27]. The parameter  $\theta_\mu \in \{\pm 1\}$  is the sign of  $\mu$  which only affects the global sign of the inferred configuration  $\vec{\sigma}^0$ . We may simply assume  $\theta_\mu = 1$  and later fix the optimal sign of  $\vec{\sigma}^0$  by energy comparison.

We should be able to achieve almost perfect inference of  $\vec{\sigma}^0$  by setting  $X \geq 5N$  [27]. The total number of sampled independent configurations is then of order  $O(N^2)$ . It may be reasonable to assume that one needs  $O(N)$  spin-flip trials to pick one independent

configuration sample, then the total time complexity of this strategy A is of order  $O(N^3)$ , much shorter than the exponential time complexity of the naive random-walk strategy.

Perfect inference is actually not necessary. We could compute the mean values of the planted spins  $\sigma_i^0$  through Eq. (9) and then use them to guide the MMC dynamics passing through the entropy valley around  $m^*$  [Fig. 3(a)].

### 5.2. Hyperplane optimization

Given  $\mathcal{N}$  independent configuration samples, the hyperplane defined by the planted configuration  $\vec{\sigma}^0$  will split these configurations into two groups such that one group contains order  $O(\mathcal{N}/\sqrt{N})$  more configurations than the other group. The hyperplane perpendicular to a random spin configuration will also split these configurations into two groups, but their size difference will only be of order  $O(\sqrt{\mathcal{N}})$ . We expect that when  $\mathcal{N}$  reaches order  $O(N^2)$  the hyperplane of the planted configuration will be the unique optimal choice to separate the  $\mathcal{N}$  configuration samples in the most uneven way. The corresponding optimization problem has the following cost function

$$\mathcal{C}(\vec{\sigma}^0) = \sum_{\ell=1}^{\mathcal{N}} \text{Sign}\left(\sum_{i=1}^N \sigma_i^{(\ell)} \sigma_i^0\right), \quad (10)$$

where  $\text{Sign}(x)$  is the sign function defined by  $\text{Sign}(x) = 1$  for  $x > 0$ ,  $\text{Sign}(x) = -1$  for  $x < 0$  and  $\text{Sign}(x) = 0$  for  $x = 0$ , and  $\sigma_i^{(\ell)}$  is the  $i$ -th entry of the  $\ell$ -th sampled configurations. The minimum-cost solution of Eq. (10) may be reachable by simulated annealing dynamics or by message-passing algorithms. The method of principal component analysis might also be helpful [29].

Both this optimization strategy (strategy B) and the perceptron-learning strategy A have the advantage that one does not need to know the value of the hyper-parameter  $\varepsilon$ . A conceptual disadvantage is that they are not applicable to problem instances with even  $p$ -values, because the overlap distribution  $P(m)$  must be symmetric when every interaction involves an even number of vertices. This disadvantage might be overcome by the strategy of the next subsection.

### 5.3. Curve-fitting strategy

The distribution  $P(m)$  of overlaps  $m$  with respective to the planted configuration  $\vec{\sigma}^0$ , viewed as a function of  $m$ , should not depend on the details of  $\vec{\sigma}^0$ . This means that we could estimate  $P(m)$  without knowing  $\vec{\sigma}^0$  simply by setting the coupling constants  $J_a$  of Eq. (1) independently as  $-1$  or  $+1$  with probabilities  $\varepsilon$  and  $1-\varepsilon$ , respectively. On the other hand, we can sample a large number of independent configurations  $\vec{\sigma}^{(\ell)} \equiv (\sigma_1^{(\ell)}, \dots, \sigma_N^{(\ell)})$ , with indices  $\ell = 1, \dots, \mathcal{N}$ , for the planted  $p$ -spin model (1) with the original set of coupling constants.

Then the following inference problem (strategy C) concerning the probability

distribution, denoted as  $P_C(\vec{\sigma}^0)$ , of the unknown planted configuration  $\vec{\sigma}^0$  arises:

$$P(m) = \frac{1}{N} \sum_{\ell=1}^N \sum_{\vec{\sigma}^0} P_C(\vec{\sigma}^0) \delta\left(m - \frac{1}{N} \sum_{i=1}^N \sigma_i^{(\ell)} \sigma_i^0\right), \quad (11)$$

where  $\delta(x)$  is the Dirac delta function. We may assume  $P_C(\vec{\sigma}^0)$  to be factorized such that

$$P_C(\vec{\sigma}^0) = \prod_{i=1}^N \left[ \frac{1 + \nu_i \sigma_i^0}{2} \right], \quad (12)$$

where  $\nu_i$  is the inferred mean value of the  $i$ -th planted entry  $\sigma_i^0$ . Then Eq. (11) can be approximated as a sum of many Gaussian distributions [27]

$$P(m) = \frac{1}{N} \sum_{\ell=1}^N \frac{1}{\sqrt{2\pi\Lambda}} \exp\left(-\frac{(m - \frac{1}{N} \sum_{i=1}^N \sigma_i^{(\ell)} \nu_i)^2}{2\Lambda}\right), \quad (13)$$

with  $\Lambda = \sum_{i=1}^N (1 - (\nu_i)^2)/N^2$  being a variance parameter.

Equation (13) is essentially a curve-fitting problem with  $N$  adjustable real parameters  $\nu_i$ . This problem may be solvable by various algorithms developed in the machine-learning community. We expect that when the number  $N$  of configuration samples becomes sufficiently large, the inferred first moments  $\nu_i$  will offer highly faithful prediction about the true planted configuration  $\vec{\sigma}^0$ .

An advantage of this inference strategy C is that it may also be applicable when the hyper-parameter  $p$  of model (1) is even-valued. For  $p$  being even, of course  $P(m)$  will be a symmetric function of  $m$ , but because configurations of larger magnitudes  $|m|$  of overlaps are more frequently to be sampled in a planted system, the form of  $P(m)$  may significantly deviate from being Gaussian, making it useful for the inference task (13).

#### 5.4. On the noise level $\varepsilon$

As mentioned in the preceding subsection, to evaluate the overlap distribution  $P(m)$  we need to discard the original coupling constants  $J_a$  of the planted model (1) and assign  $\pm 1$  values to them according to the noise level  $\varepsilon$ . But the value of this hyper-parameter  $\varepsilon$  may often be unknown.

This lack of information should not cause a fundamental difficulty. We may simply set  $\varepsilon$  to a set of different values between 0 and  $\frac{1}{2}$ . For each fixed value of  $\varepsilon$  we can get the corresponding  $P(m)$  function and use it as input to the inference problem (13), while the set of configuration samples  $\vec{\sigma}^{(\ell)}$  is the same. We may be able to achieve the best fitting performance when the assigned  $\varepsilon$  is close to the true value of this noise level.

## 6. Summary

In summary, we picked the  $p$ -spin interaction model as an example to demonstrate the potential of microcanonical spontaneous symmetry breaking for solving hard inference

problems; and we conjectured that machine-learning methods such as perceptron learning could serve as promising strategies to achieve MSSB and retrieve the planted ground state within  $O(cN^3)$  elementary localized updates, possibly with a large prefactor  $c$ .

The finite-size scaling behaviors (7) and (8) are quite fascinating and they call for a thorough theoretical understanding. Numerical implementation of the three machine-learning strategies of Section 5 will be needed to check the validity of our conjecture. We are also starting to work on other challenging planted ensembles of optimization problems, such as  $K$ -satisfiability and  $Q$ -coloring [12, 14, 13], to get more insights on the MSSB mechanism.

## Acknowledgments

The author thanks Yuliang Jin and Pan Zhang for helpful conversations. This work was supported by the National Natural Science Foundation of China Grants No.11975295 and No.11947302, and the Chinese Academy of Sciences Grant No.QYZDJ-SSW-SYS018. Numerical simulations were carried out at the Tianwen clusters of ITP-CAS and the Tianhe-2 platform of the National Supercomputer Center in Guangzhou.

## Appendix A. Additional numerical results

The mean-field theoretical results obtained for the planted 3-body spin model on a regular random network of degree  $K = 4$  are summarized in Fig. A1. Qualitatively speaking, these theoretical results are identical to the results shown in Fig. 2 for  $K = 10$ . The circles in Fig. A1(c) are simulation results obtained on a single network instance of size  $N = 10002$ . Because of the huge entropy barrier and the large gap of the order parameter  $m$  between the DS and MP phases, the waiting time to observe a MSSB transition is too much longer than the simulation time, and consequently such a transition does not occur in our simulation processes.

Figure A2 shows how the asymmetry of the probability distribution  $P(m)$  changes with the energy density  $u$ , for a single random-network instance of degree  $K = 4$  and size  $N = 4008$ . From the fact that the different curves superimpose onto each other after rescaling the probability distributions by  $|u|$  [Fig. A2(b)], we know that the asymmetry of  $P(m)$  decreases linearly with  $|u|$  and vanishes as  $u$  approaches zero.

We show in Fig. A3 the probability profiles of the overlap  $m$  in the vicinity of  $m = 0$  for single RR network instances of degree  $K = 10$ . These results are obtained by sampling a huge number of spin configurations at fixed energy density  $u = -1.61$  through the MMC evolution dynamics. This figure confirm that the asymmetric features revealed in Fig. 4(a) are quite general for RR networks of different degrees  $K$ . For the system of size  $N = 15360$ , we estimate the asymmetry parameters to be  $\mu = 0.223 \pm 0.006$  and  $\lambda = 1.112 \pm 0.006$ , and  $m_0 = 0.00028$  (the number of configuration samples is  $\mathcal{N} = 4.8 \times 10^8$  for this problem instance).

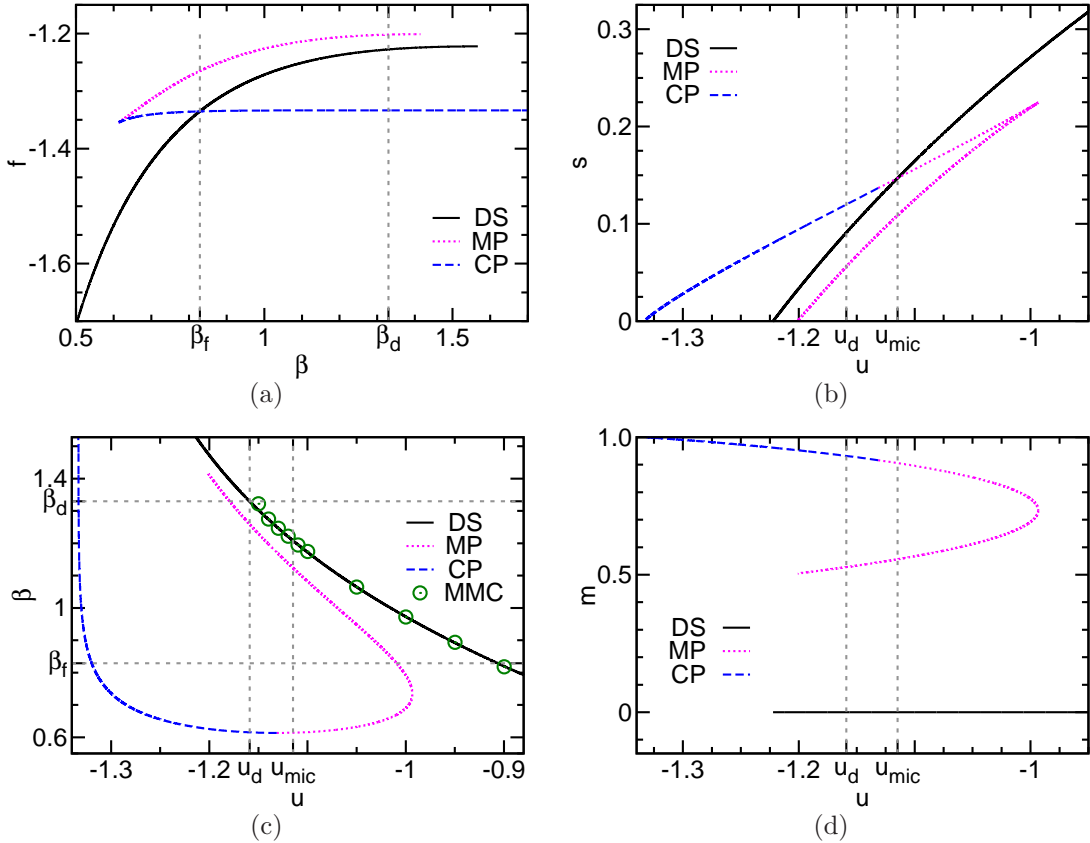


**Figure A1.** The DS (solid lines), MP (dotted lines), and CP (long dashed lines) fixed points of the mean-field theory for the planted 3-body model on random graphs of degree  $K = 4$  (noise  $\varepsilon \rightarrow 0$ ). (a) Free energy density  $f$  versus canonical inverse temperature  $\beta$ . (b) Entropy density  $s$  versus energy density  $u$ . (c) Microcanonical inverse temperature  $\beta$  versus  $u$ . Circular symbols are MMC simulation results obtained on a single problem instance of size  $N = 10002$ . (d) Mean overlap  $m$  versus  $u$ .  $\beta_d$  and  $u_d$ : critical inverse temperature and energy density at the dynamical SG phase transition;  $u_{\text{mic}}$ : critical energy density at the MSSB phase transition;  $\beta_f$ : critical inverse temperature at the canonical ferromagnetic phase transition.

## Appendix B. Bootstrap statistics analysis

We estimate the statistical errors of the scaling coefficients  $\lambda$  and  $\mu$  of Eqs. (7) and (8) by the bootstrap method [18, 30].

Consider a random variable  $x$  which can take  $m$  different values  $x_1, \dots, x_m$ . We are given a large number  $\mathcal{N}$  of independent samples of this random number, among which  $n_i$  samples are the value  $x_i$  ( $n_i \geq 0$  for  $i = 1, \dots, m$  and  $\sum_{i=1}^m n_i = \mathcal{N}$ ). An empirical mean of this random variable is then constructed as

$$\bar{x} = \frac{1}{\mathcal{N}} \sum_{i=1}^m n_i x_i. \quad (\text{B.1})$$

Because the sample set size  $\mathcal{N}$  is finite, the empirical mean  $\bar{x}$  may deviate from the true mean of the random variable  $x$ .

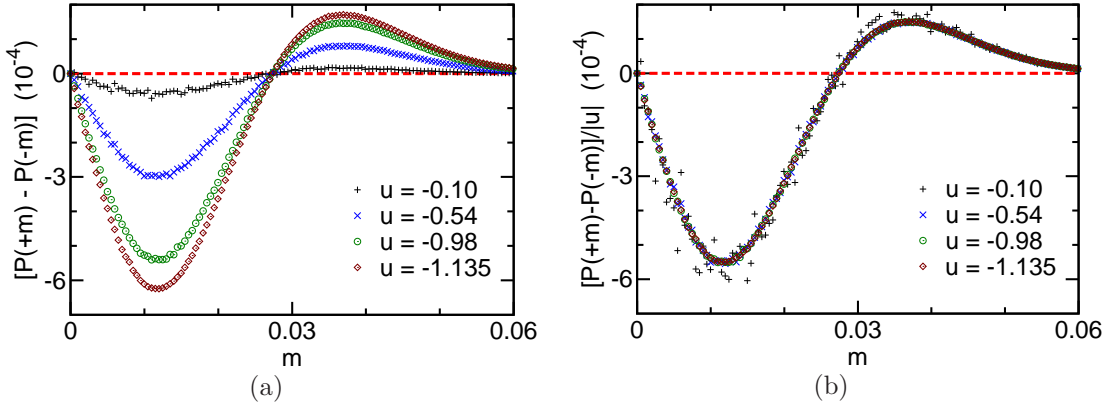


**Figure A2.** Probability difference (unit  $10^{-4}$ ) between positive and negative overlap values  $m$  in a single random-network system of  $K=4$  and  $N=4008$ . The energy density is  $u=-0.10$  (pluses),  $-0.54$  (crosses),  $-0.984$  (circles), and  $-1.135$  (diamonds). Panel (b) is rescaled plot of panel (a) with the vertical axis being the ratio between the probability difference and  $|u|$ .

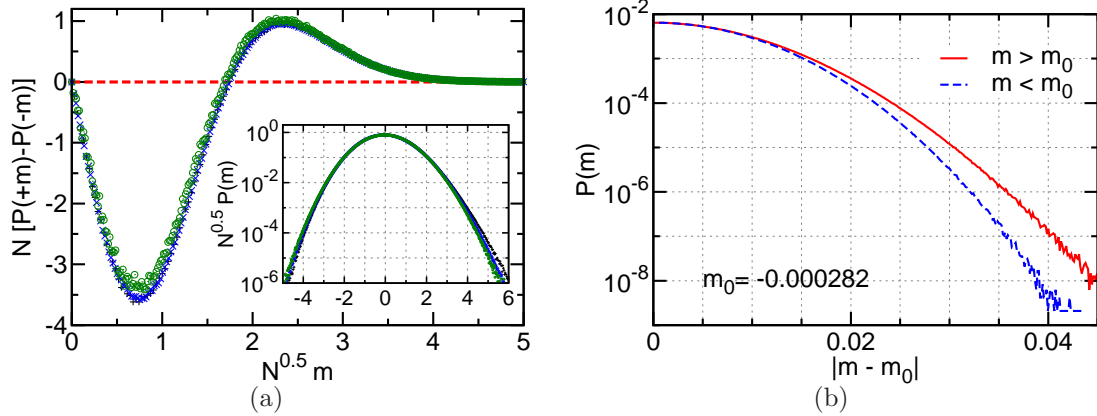


**Figure A3.** Asymmetry of the overlap distribution  $P(m)$  for the planted 3-body model on single random graphs of degree  $K=10$  at noise  $\varepsilon=0$ . (a) Rescaled probability difference  $N[P(+|m|) - P(-|m|)]$  versus rescaled overlap  $\sqrt{N}m$  at  $u=-1.61$ : size  $N=3840$  (pluses),  $7680$  (crosses),  $15360$  (circles). The inset shows  $\sqrt{N}P(m)$  versus  $\sqrt{N}m$ . (b) The two branches of  $P(m)$  at  $m > m_0$  and  $m < m_0$  for the system of size  $N=15360$ , with  $m_0=-0.000282$  being the most probable overlap value.

To estimate the standard error of the empirical mean, we assume that the true probability distribution of  $x$  is identical to the empirical distribution, namely the probability of  $x = x_i$  is  $p_i = n_i/\mathcal{N}$ . It then follows that the joint probability  $P(n_1, \dots, n_m)$  that, among  $\mathcal{N}$  independent samples,  $n_i$  of them equal to  $x_i$  is

$$P(n_1, \dots, n_m) = \frac{\mathcal{N}!}{n_1! \dots n_m!} p_1^{n_1} \dots p_m^{n_m}. \quad (\text{B.2})$$

According to this probability distribution, the first moments  $\langle n_i \rangle$  and the correlations  $\langle n_i n_j \rangle$  of these random counting numbers  $n_i$  are simply

$$\langle n_i \rangle = \mathcal{N} p_i, \quad \langle n_i n_j \rangle = \mathcal{N}(\mathcal{N}-1) p_i p_j + \mathcal{N} p_i \delta_i^j, \quad (\text{B.3})$$

where  $\delta_i^j = 0$  if  $i \neq j$  and  $\delta_i^j = 1$  if  $i = j$ . Then, the standard deviation of the empirical mean  $\bar{x}$  is

$$SD(\bar{x}) \equiv \sqrt{\langle(\bar{x})^2\rangle - \langle\bar{x}\rangle^2} = \left(\frac{\bar{x}^2 - \langle\bar{x}\rangle^2}{\mathcal{N}}\right)^{\frac{1}{2}}, \quad (\text{B.4})$$

where  $\bar{x}^2$  is the empirical second moment of  $x$ :

$$\bar{x}^2 = \frac{1}{\mathcal{N}} \sum_{i=1}^m n_i x_i^2. \quad (\text{B.5})$$

Applying the above statistical theory to the parameter  $\lambda$ , we notice that the random variable in this case is  $x \in \{-\sqrt{N}, 0, +\sqrt{N}\}$  corresponding to the overlap value  $m$  being positive, zero, and negative, respectively. Then the standard deviation of  $\lambda$  is

$$SD(\lambda) \approx \sqrt{\frac{N}{\mathcal{N}}}. \quad (\text{B.6})$$

For the parameter  $\mu$ , the corresponding random variable is  $x = \sum_{i=1}^N \sigma_i \sigma_i^0$  where  $\sigma_i$  is the spin of vertex  $i$  in the sampled configuration  $\vec{\sigma}$ . Then the standard deviation of  $\mu$  is

$$SD(\mu) \approx \sqrt{\frac{N}{\mathcal{N}}}. \quad (\text{B.7})$$

We see that the standard errors of  $\lambda$  and  $\mu$  both are approximately  $\sqrt{N/\mathcal{N}}$ .

## References

- [1] S. Franz, M. Mézard, F. Ricci-Tersenghi, M. Weigt, and R. Zecchina. A ferromagnet with a glass transition. *Europhys. Lett.*, 55:465–471, 2001.
- [2] A. Montanari and F. Ricci-Tersenghi. Cooling-schedule dependence of the dynamics of mean-field glasses. *Phys. Rev. B*, 70:134406, 2004.
- [3] L. Zdeborová and F. Krzakala. Statistical physics of inference: thresholds and algorithms. *Adv. Phys.*, 65:453–552, 2016.
- [4] M. Mézard and A. Montanari. *Information, Physics, and Computation*. Oxford Univ. Press, New York, 2009.
- [5] N. Sourlas. Spin-glass models as error-correcting codes. *Nature*, 339:693–695, 1989.
- [6] H. Huang and H. J. Zhou. Cavity approach to the Sourlas code system. *Phys. Rev. E*, 80:056113, 2009.
- [7] O. Watanabe. Message passing algorithms for MLS-3LIN problems. *Algorithmica*, 66:848–868, 2013.
- [8] S. Kirkpatrick, C. D. Gelatt Jr., and M. P. Vecchi. Optimization by simulated annealing. *Science*, 220:671–680, 1983.
- [9] Y.-Z. Xu, C. H. Yeung, H.-J. Zhou, and D. Saad. Entropy inflection and invisible low-energy states: Defensive alliance example. *Phys. Rev. Lett.*, 121:210602, 2018.
- [10] Y. Matsuda, H. Nishimori, L. Zdeborová, and F. Krzakala. Random-field  $p$ -spin-glass model on regular random graphs. *J. Phys. A: Math. Theor.*, 44:185002, 2011.
- [11] A. S. Bandeira, A. Perry, and A. S. Wein. Notes on computational-to-statistical gaps: Predictions using statistical physics. *Portugaliae Mathematica*, 75:159–186, 2018.
- [12] K. Li, H. Ma, and H. J. Zhou. From one solution of a 3-satisfiability formula to a solution cluster: Frozen variables and entropy. *Phys. Rev. E*, 79:031102, 2009.
- [13] F. Krzakala, M. Mézard, and L. Zdeborová. Reweighted belief propagation and quiet planting for random  $k$ -sat. *Journal on Satisfiability, Boolean Modeling and Computation*, 8:149–171, 2014.

- [14] F. Krzakala and L. Zdeborová. Hiding quiet solutions in random constraint satisfaction problems. *Phys. Rev. Lett.*, 102:238701, 2009.
- [15] H.-J. Zhou. Kinked entropy and discontinuous microcanonical spontaneous symmetry breaking. *Phys. Rev. Lett.*, 122:160601, 2019.
- [16] M. Mézard and G. Parisi. The Bethe lattice spin glass revisited. *Eur. Phys. J. B*, 20:217–233, 2001.
- [17] M. Mézard and A. Montanari. Reconstruction on trees and spin glass transition. *J. Stat. Phys.*, 124:1317–1350, 2006.
- [18] H.-J. Zhou. *Spin Glass and Message Passing*. Science Press, Beijing, China, 2015.
- [19] D. H. E. Gross. *Microcanonical Thermodynamics: Phase Transitions in “Small” Systems*. World Scientific, Singapore, 2001.
- [20] M. Creutz. Microcanonical Monte Carlo simulation. *Phys. Rev. Lett.*, 50:1411–1414, 1983.
- [21] G. H. Weiss. First passage time problems for one-dimensional random walks. *J. Stat. Phys.*, 24:587–594, 1981.
- [22] M. Khantha and V. Balakrishnan. First passage time distribution for finite one-dimensional random walks. *Pramana*, 21:111–122, 1983.
- [23] A. Engel and C. Van den Broeck. *Statistical Mechanics of Learning*. Cambridge University Press, Cambridge, UK, 2001.
- [24] Y. Kabashima and S. Uda. A BP-based algorithm for performing bayesian inference in large perceptron-type networks. *Lect. Notes Artif. Intellig.*, 3244:479–493, 2004.
- [25] A. Braunstein and R. Zecchina. Learning by message passing in networks of discrete synapses. *Phys. Rev. Lett.*, 96:030201, 2006.
- [26] H. Huang and T. Toyoizumi. Advanced mean-field theory of the restricted Boltzmann machine. *Phys. Rev. E*, 91:050101(R), 2015.
- [27] H.-J. Zhou. Active online learning in the binary perceptron problem. *Commun. Theor. Phys.*, 71:243–252, 2019.
- [28] H. Bauke and S. Mertens. Random numbers for large-scale distributed monte carlo simulations. *Phys. Rev. E*, 75:066701, 2007.
- [29] G.-K. Hu, T. Liu, M.-X. Liu, W. Chen, and X.-S. Chen. Condensation of eigen microstate in statistical ensemble and phase transition. *Science China Phys. Mech. Astron.*, 62:990511, 2019.
- [30] B. Efron. Computers and the theory of statistics: Thinking the unthinkable. *SIAM Rev.*, 21:460–480, 1979.